Article:
Zhang, G., Xu, H., Wu, D. et al. (4 more authors) (2025) Relationship investigation between quantitative cellular information and self-acceleration of lean hydrogen-air spherical premixed flame. Energy, 325. 136175. ISSN 0360-5442

https://doi.org/10.1016/j.energy.2025.136175

Energy

Relationship investigation between quantitative cellular information and self-acceleration of lean hydrogen-air spherical premixed flame

--Manuscript Draft--

Manuscript Number:	EGY-D-25-03212
Article Type:	Full length article
Section/Category:	Energy and Transportation
Keywords:	Hydrogen; Premixed combustion; Instability; Spherical flame; Self-acceleration
Corresponding Author:	GENGXIN ZHANG University of Birmingham BIRMINGHAM, UK UNITED KINGDOM
First Author:	GENGXIN ZHANG
Order of Authors:	GENGXIN ZHANG
	Hongming Xu
	Dawei Wu
	Junfeng Yang
	Mohamed E. Morsy
	Mehdi Jangi
	Roger Cracknell
Abstract:	Due to the high diffusivity of hydrogen molecules, lean hydrogen-air premixed flames are more prone to cellular instability during combustion. This instability is known to often lead to self-acceleration of flame propagation, with the flame speed closely related to the cellular area on its surface. In this study, the relationship between quantitative cellular information and self-acceleration of lean hydrogen-air premixed spherically expanding flames was systematically analyzed under various initial temperatures. Quantitative cellular information was obtained using an in-house developed image processing program. Based on these quantitative data, the ratio of cellular flame surface area to laminar flame surface area was calculated, and the fractal dimension of the flame front along with the flame self-acceleration exponent was derived. Results indicate that with increasing equivalence ratio and initial temperature, the onset of cellular instability is delayed, while the self-acceleration exponent gradually increases with flame propagation, eventually stabilizing in the range of 1.2-1.4 after full cellularization. Under leaner conditions and lower initial temperatures, flames exhibited a higher self-acceleration exponent. The self-acceleration exponent obtained from the 3D-reconstructed cellular flame area offers a new perspective for developing accurate models of self-accelerating spherically cellular flame propagation, with significant potential applications in hydrogen combustion and explosion safety.

Declaration of interests

☒The authors declare that they have no known competing financial interests or personal relationships that could have appeared to influence the work reported in this paper.

☐The authors declare the following financial interests/personal relationships which may be considered as potential competing interests:

Highlights

- The self-acceleration of lean hydrogen-air flames under various temperatures was studied
- The quantitative relationship between self-acceleration and flame surface data was explored
- The self-acceleration exponent of cellular flames increases progressively during propagation
- The self-acceleration exponent derived from 3D cellular flame area stabilizes at 1.2-1.4

Graphical Abstract

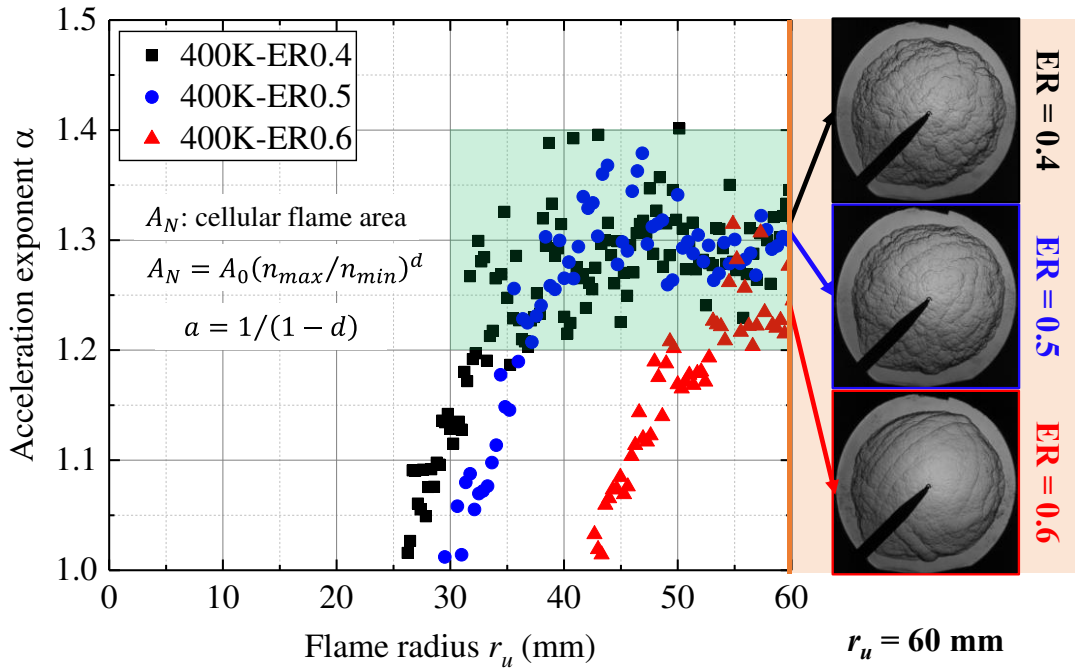

Relationship investigation between quantitative cellular information and self-acceleration of lean hydrogen-air spherical premixed flame

Authors:

Gengxin Zhang [a], Hongming Xu [a] *, Dawei Wu [a], Junfeng Yang [b], Mohamed E. Morsy [b], Mehdi Jangi [a], Roger Cracknell [c]

[a] Department of Mechanical Engineering, School of Engineering, University of Birmingham, Edgbaston, Birmingham B15 2TT, UK

[b] School of Mechanical Engineering, University of Leeds, Leeds LS2 9JT, UK

[c] Shell Global Solutions UK, Shell Centre, London SE1 7NA, UK

*Corresponding author:

E-mail address: h.m.xu@bham.ac.uk (Hongming Xu)

Abstract

Due to the high diffusivity of hydrogen molecules, lean hydrogen-air premixed flames are more prone to cellular instability during combustion. This instability is known to often lead to self-acceleration of flame propagation, with the flame speed closely related to the cellular area on its surface. In this study, the relationship between quantitative cellular information and self-acceleration of lean hydrogen-air premixed spherically expanding flames was systematically analyzed under various initial temperatures. The focus was on equivalence ratios of 0.4, 0.5, and 0.6, with initial temperatures set at 300 K, 360 K, and 400 K. Quantitative cellular information, including cell number, two- and three-dimensional average cell area, and total cellular flame area, was obtained using an in-house developed image processing program.

Based on these quantitative data, the ratio of cellular flame surface area to laminar flame surface area was calculated, and the fractal dimension of the flame front along with the flame self-acceleration exponent was derived. Results indicate that with increasing equivalence ratio and initial temperature, the onset of cellular instability is delayed, while the self-acceleration exponent gradually increases with flame propagation, eventually stabilizing in the range of 1.2-1.4 after full cellularization. Under leaner conditions and lower initial temperatures, flames exhibited a higher self-acceleration exponent. The self-acceleration exponent obtained from the 3D-reconstructed cellular flame area offers a new perspective for developing accurate models of self-accelerating spherically cellular flame propagation, with significant potential applications in hydrogen combustion and explosion safety.

Keywords: Hydrogen, Premixed combustion, Instability, Spherical flame, Self-acceleration

1 Introduction

Hydrogen is a renewable energy source that can be produced sustainably, with the advantage of emitting no greenhouse gases when burned in air [1,2]. Meanwhile, hydrogen has certain unique characteristics, such as low ignition energy, a wide flammability range, and high diffusivity, which can pose significant risks of fire or explosion [3-5]. Additionally, lean fuel mixtures are particularly attractive in combustion systems, as they reduce flame temperature, thereby lowering thermal stress on combustion chamber walls, reducing fuel consumption, and decreasing NOx

emissions [6, 7]. However, the hydrogen-air combustion process under lean conditions is inherently unstable. Specifically, spherically propagating premixed hydrogen-air flames are prone to phenomena such as cellularization, self-acceleration, self-similarity, and even transition to self-turbulence. These instabilities in flame propagation pose serious threats to the safety and reliability of combustion equipment [8-10]. Therefore, it is crucial to study the instability behavior of near-limit lean hydrogen-air flames to ensure safe and reliable operation of combustion systems running on lean mixtures.

A key question in the propagation of self-similar spherically expanding flames is the self-acceleration exponent, often estimated by the power-law relationship $r_u \sim t^a$. Gostintsev et al. found the flame radius self-acceleration exponent to be 1.5, which they identified as the threshold for flame self-turbulence [11]. Subsequently, other researchers have further studied the self-acceleration exponent of expanding flames for various fuels, obtaining values consistent with Gostintsev's 1.5 [12, 13]. Bradley et al. investigated the acceleration behavior of stoichiometric methane flames (equivalence ratio = 1.1) and propane flames (equivalence ratio = 1.06) under ambient temperature and pressure using large-scale constant volume combustion vessels, finding self-acceleration exponent similar to those obtained by Gostintsev as well [14]. Kwon et al. also analyzed the self-acceleration of hydrogen flames under different combustion conditions in their studies on flame instability, reporting self-acceleration exponents between 1.23 and 1.36, which are lower than 1.5. They noted that the acceleration of spherically expanding flames remains a topic requiring further clarification [15]. Additionally, Gostintsev et al. revised their original conclusions in their later studies,

finding that the flame self-acceleration exponent was actually lower than the previously estimated 1.5, highlighting further uncertainty in understanding the self-acceleration exponent [16]. Recently, several small-scale [17-23] and large-scale field experiments [24-26] have shown that the self-acceleration exponent generally falls within the range of 1.1~1.4. Kim et al. observed that the value of the self-acceleration exponent increases with flame radius and eventually saturates at a critical value corresponding to the fractal dimension. In other words, a transitional state exists before the large-scale expanding flame reaches self-turbulence [24]. Cai et al. introduced two different acceleration exponents: the transitional and the self-similar acceleration exponents. They also proposed a potential empirical power-law correlation to capture the entire self-acceleration process [27]. However, to date, there is no unified, precise conclusion regarding the self-acceleration characteristics of expanding flames. Moreover, localized cascade mechanisms within cellular structures may lead to fluctuations in surface area, with alternating phases of rapid and slow growth, resulting in a global pulsating mode that the classic power-law relationship cannot capture [28, 29].

Based on the literature review above, no studies to date have examined the relationship between the actual cellular flame area and flame self-acceleration under lean combustion conditions. This study aims to experimentally investigate the propagation of lean premixed spherically expanding hydrogen-air flames under different initial temperatures, focusing on quantitatively analyzing flame instability and the self-acceleration exponent from the perspective of cellular flame area. The organization of this work is as follows: first, the Schlieren optical diagnostics were used

to capture images of spherically expanding flames under various low equivalence ratios; then, an in-house developed image processing program was applied to segment cellular structures on the flame surface and reconstruct the flame area in 3D; finally, a quantitative analysis was conducted to explore the relationship between the self-acceleration exponent of unstable spherically expanding flames and their cellular flame area.

2 Experimental Equipment and Methods

To capture images of the spherically propagating premixed flames of lean hydrogen-air mixtures, Schlieren optical diagnostics was employed in this study, as shown in Figure 1. The spherical constant volume combustion chamber has an inner diameter of 380 mm and is equipped with two pairs of circular optical windows, each 150 mm in diameter, to allow observation of flame propagation. Additionally, four fans were installed at the corners of the combustion chamber to ensure uniform mixing of fuel and air. To achieve non-turbulent premixed combustion, the fans were used to homogenize the fuel-air mixture, and ignition was delayed for at least 15 seconds after mixing. The ignition system, located at the center of the chamber, consists of a standard 12V transistorized automotive ignition coil that provides an ignition energy of approximately 1 mJ. Furthermore, two 2 kW electric heaters were installed on the chamber walls to heat the mixture, ensuring the desired initial temperature conditions.

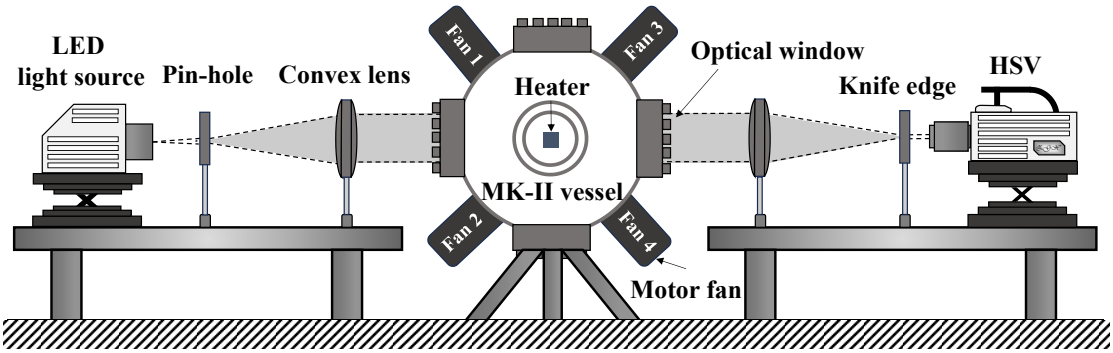

Fig. 1. Optical diagnostic arrangement for spherical premixed flame observation.

In this study, to investigate the propagation characteristics of spherically expanding lean hydrogen-air premixed flames under different initial temperatures, the initial temperatures were set at 300 K, 360 K, and 400 K, with equivalence ratios of 0.4, 0.5, and 0.6. A high-speed imaging system was employed to capture the flame propagation at a frame rate of 30,000 fps and a spatial scale of 0.27 mm/pixel, resulting in 768×768 resolution flame images for subsequent analysis.

After obtaining images of the spherically expanding flame propagation, an in-house developed image processing code was used to segment the cells on the flame surface, extracting quantitative cellular information, including cell number, centroid position, and two-dimensional (2D) average area [30]. Subsequently, a three-dimensional (3D) reconstruction of the area for all cells distributed on the flame surface was conducted to calculate the cellular flame area [31]. Additional flame features, such as flame contour and equivalent radius, were also extracted at the same time. Details of the image processing logic and uncertainty analysis for the processing steps can be found in our previous publications [30, 31].

3 Results and Discussion

3.1 Basic flame characteristics and instability analysis

Figure 2 shows the evolution of raw images of spherical flame propagation under various initial temperatures and fuel-air equivalence ratios. The equivalent flame radius r_u was obtained through image processing and is defined as $r_u = \sqrt{A/\pi}$, where A is the flame area determined by the sum of pixels of binarized flame image. Due to the limitations of the optical window in the constant volume combustion chamber, the maximum flame radius measurable in this study is approximately 60 mm.

As shown in the figure, the flame front appears relatively smooth at smaller flame radius ($r_u < 15$ mm), primarily because the high stretch rate at this stage suppresses the rapid formation of cellular structures, helping to maintain flame stability. However, at the initial moment, interference from the electrodes causes noticeable large cracks on the flame surface. With increasing equivalence ratio and initial temperature, the relative impact of electrode interference on the initial flame morphology gradually decreases, and the flame surface exhibits a smoother spherical shape at small radius. As the flame continues to propagate, secondary cracks begin to appear, with smaller branches forming on the initial large cracks, eventually leading to a flame surface covered in cells of varying sizes. The formation of these cellular structures is mainly attributed to the interaction between thermal-diffusive and hydrodynamic instabilities [32]. Given the relatively small spatial scale in this study, the effect of buoyancy-induced instability is negligible under these conditions. The development of cellular structures is known to contribute to the self-acceleration of flame propagation. Observations show that, with increasing initial temperature and fuel-air equivalence ratio, the degree of

cellularization in lean flames tends to decrease. This variation in cellularization is clearly visible in the raw schlieren images, reflecting the instability evolution patterns of lean flames under different conditions.

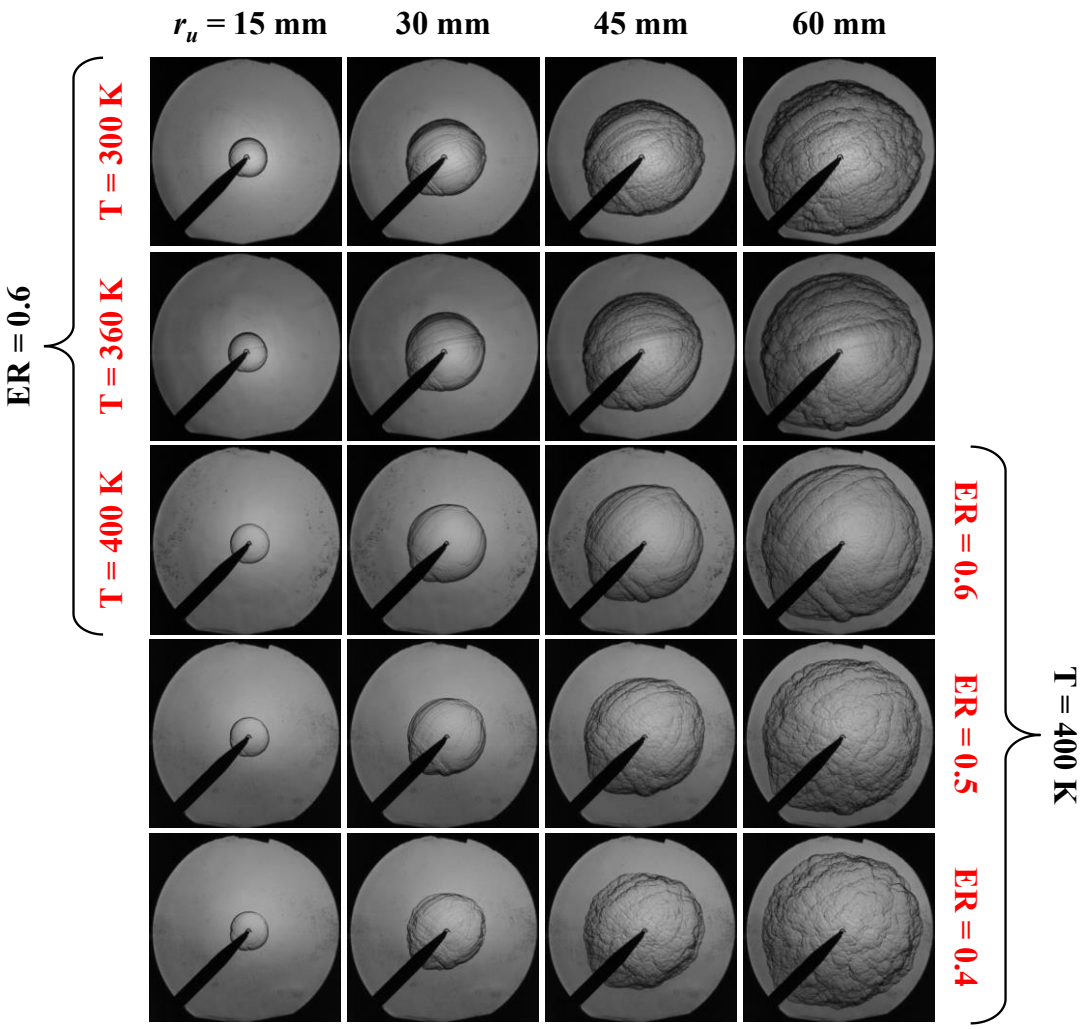

Fig. 2. Premixed combustion spherical flame propagation at various temperatures under lean combustion conditions.

In the propagation of spherically expanding flames, the flame is continuously influenced by stretch, resulting in changes in its surface area, which in turn affects the flame propagation speed. The flame stretch rate α is defined as the rate of change in surface area due to spherical expansion of the flame front. Its expression is given in Equation (1), where the stretched flame speed is defined as $S_n = dr_u/dt$ [33]:

$$\alpha = \frac{1}{A}\frac{dA}{dt} = \frac{1}{4\pi {r_u}^2}\frac{d(4\pi {r_u}^2)}{dt} = \frac{2}{r_u}\frac{dr_u}{dt} = \frac{2}{r_u}S_n \quad (1)$$

Figure 3 illustrates the variation of flame stretch rate with equivalent flame radius under various lean combustion conditions. Figures 3 (a) and 3 (b) specifically show the influence of fuel-air equivalence ratio and initial temperature on the stretch rate, respectively. The results indicate that as the flame radius increases, the stretch rate decreases approximately as a power-law function, with the rate of decrease accelerating with an increase in the fuel-air equivalence ratio. The effect of initial temperature variation is relatively minor. Overall, higher initial temperatures and greater initial equivalence ratios result in higher stretch rates. At the early stages of combustion, higher stretch rates suppress flame instability, whereas, in later stages, as the stretch rate gradually decreases, the flame increasingly exhibits cellular structures and becomes more unstable. This phenomenon highlights the significant impact of stretch on flame instability: at higher stretch rates, the flame structure remains relatively smooth, whereas, at lower stretch rates, thermal-diffusive and hydrodynamic instabilities become more pronounced, leading to cellularization of the flame surface.

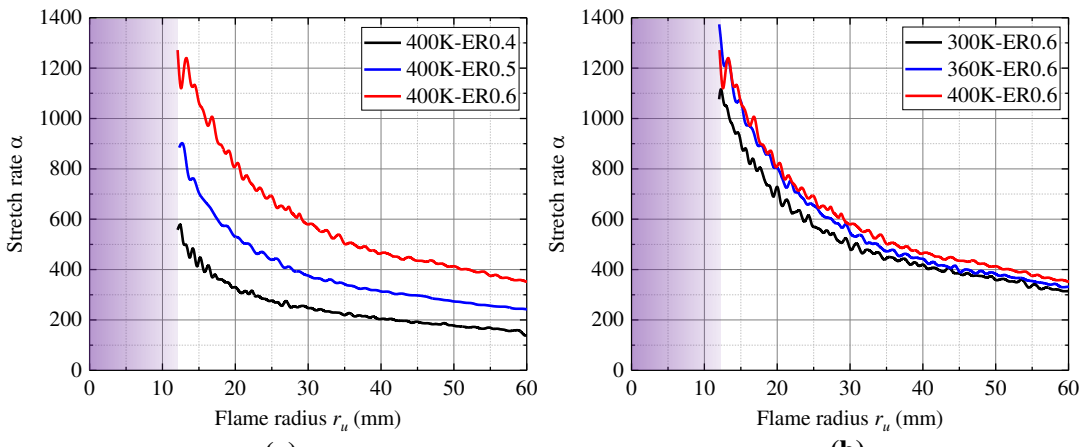

Fig. 3. Flame stretch rate at various temperatures under lean combustion conditions.

Figure 4 shows the stretched flame propagation speed under various lean combustion conditions, with Figures 4 (a) and (b) specifically illustrating the relationship between stretched flame propagation speed and flame stretch rate for different fuel-air equivalence ratios and initial temperatures in hydrogen-air combustion, respectively. As seen in the figure, the stretched flame propagation speed exhibits fluctuations during the initial ignition phase due to the influence of ignition energy [34]. Once the ignition effect diminishes, a clear linear relationship emerges between the stretched flame propagation speed and the stretch rate. This linear relationship has been confirmed through theoretical analysis, numerical simulations, and experimental methods [34-36]. The specific expression is given in Equation (2), where S_L denotes the unstretched flame propagation speed, and L_b represents the Markstein length:

$$S_L - S_n = L_b \cdot \alpha \tag{2}$$

As indicated by Equation (2), the slope of the linear fit of S_n versus α is $-L_b$. When $L_b = 0$, α has no influence on S_n; When $\alpha = 0$, $S_L = S_n$, meaning that the intersection of the extrapolated linear relationship at $\alpha = 0$ yields the value of S_L. The unstretched flame propagation speeds S_L determined under various lean combustion conditions are labeled in Figure 4, showing an increase with higher initial equivalence ratios and a slight increase with higher initial temperatures. As the flame expands beyond the critical cellular radius (inflection point), cellular structures begin to appear on the flame front, and the propagation speed then increases significantly. The results also indicate that stretched flame propagation speed increases with both initial equivalence ratio and temperature, although it shows relatively low sensitivity to

temperature changes.

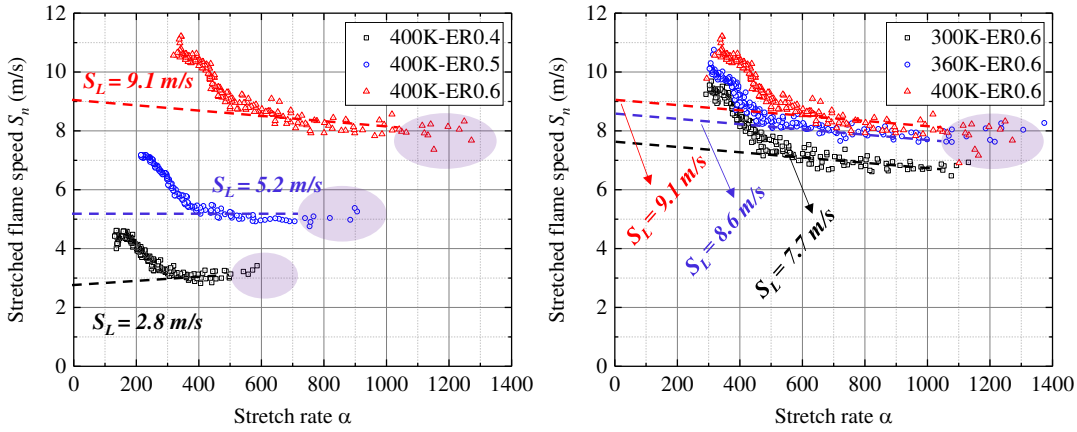

Fig. 4. Stretched flame speed at various temperatures under lean combustion conditions.

As the flame becomes thinner, its density gradient increases, making flame thickness a key factor in determining flame hydrodynamic stability. Flame thickness typically refers to the distance between the burned and unburned regions, representing the combined width of the preheat zone and the reaction zone. One common method for calculating flame thickness is based on the flame temperature profile, as expressed in Equation (3) [37], T_{ad} denotes the adiabatic flame temperature, T_u represents the unburned mixture temperature, and $(dT/dx)_{max}$ is the maximum temperature gradient:

$$\delta_T = \frac{T_{ad} - T_u}{(dT/dx)_{max}} \tag{3}$$

The above definition of flame thickness is only applicable to flames with a chemically inert preheat zone, such as methane, propane, ethylene, and acetylene flames, where this definition can be easily related to the classical definition of flame thickness. However, recent studies have indicated that the applicability of traditional equations to hydrogen flames is questionable, as the fundamental assumption of a chemically inert preheat zone does not hold in this case [38]. In laminar flames, H atoms

rapidly diffuse toward the leading edge, where they trigger reactions much more intensely than in hydrocarbon flames, resulting in a significantly reduced preheat zone. Therefore, the preheat zone flame thickness discussed in this study is determined by the following expression [39]:

$$\delta_k = \frac{(k/c_p)_{T^0}}{\rho_u S_L} \tag{4}$$

where $(k/c_p)_{T^0}$ is the ratio of thermal conductivity and specific heat at a certain inner layer temperature T^0. The values of T^0 for different gases are presented in [39].

As shown in Figure 5, the results indicate that with an increasing equivalence ratio, flame thickness decreases, while an increase in initial temperature has little effect in flame thickness. This suggests that the hydrodynamic stability of lean flames decreases with higher equivalence ratios but remains unchanged with increasing initial temperatures.

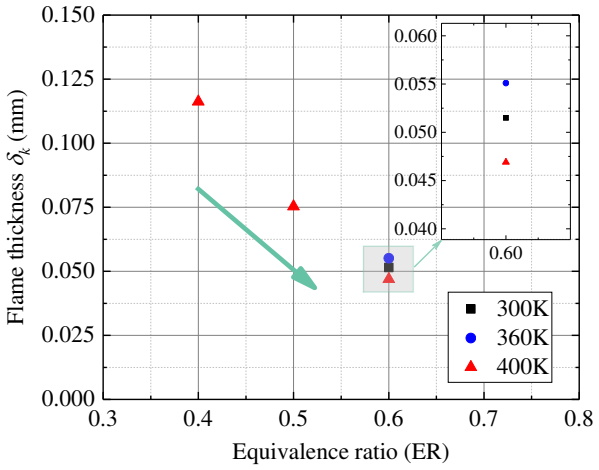

Fig. 5. Flame thickness at various temperatures under lean combustion conditions.

The Markstein length can be used to describe the stability and sensitivity of the flame front in premixed combustion, reflecting the flame's responsiveness to fluid flow or disturbances. Under lean combustion conditions, the sensitivity of Markstein length

to changes in fuel concentration is more pronounced [40]. The Markstein length can be derived inversely from the relationship for unstretched flame propagation speed (Equation 2), and the experimentally measured Markstein lengths are shown in Figure 6 (a). The results indicate that Markstein length increases with the initial equivalence ratio but is relatively insensitive to changes in initial temperature. The Markstein number M_{ab} is a dimensionless parameter that relates flame propagation speed to its sensitivity to curvature, providing a measure of flame stability. It is defined as the ratio of Markstein length to flame thickness, with the calculation shown in Equation (5). A positive Markstein number indicates stability to curvature perturbations, while a negative Markstein number implies instability. The smaller the Markstein number, the earlier the flame becomes unstable and tends to cellularize [41].

$$M_{ab} = L_b/\delta_k \tag{5}$$

The Markstein number can be determined using the flame thickness δ_k obtained from Eq. (4), as shown in Figure 6 (b). The results indicate that the trend in Markstein number with changes in initial equivalence ratio and temperature is consistent with that of the Markstein length. From the figure, it can be observed that at an initial temperature of 400 K, the Markstein number approaches zero when the equivalence ratio is close to 0.5. For equivalence ratios ER<0.5, the Markstein number becomes negative, indicating that hydrogen-air premixed flames exhibit high instability to curvature perturbations under ultra-lean conditions, making the flame surface more prone to cellular structures.

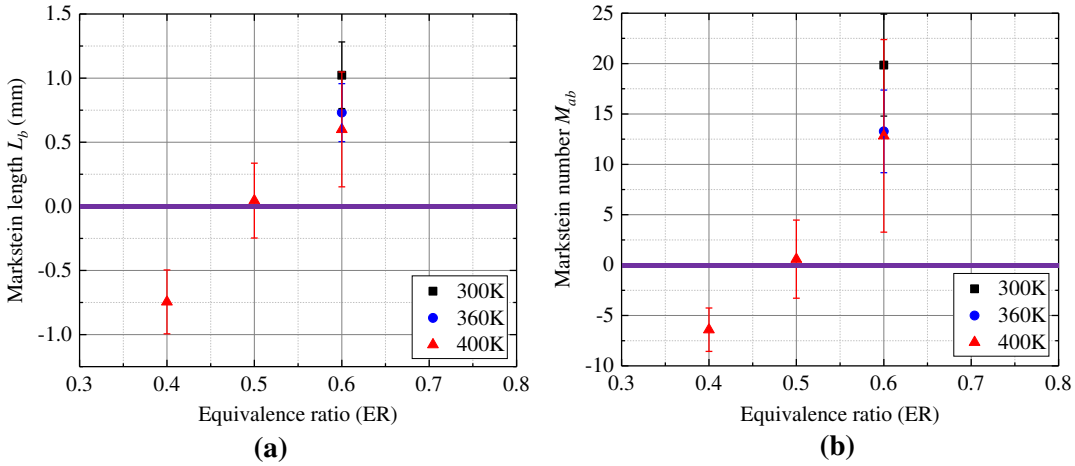

Fig. 6. Markstein length and number at various temperatures under lean combustion conditions.

Bechtold et al. successfully analyzed the transition of spherically expanding flames to a cellular instability state, finding that the Peclet number P_e plays an important role in describing the evolution of flame instability [42, 43]. The dimensionless Peclet number is defined as the ratio of flame radius to corresponding flame thickness, $P_e = r_u/\delta_k$.

Figures 7 (a) and (b) show the variation of Peclet number over time under various fuel-air equivalence ratios and initial temperature conditions, respectively. The results indicate that, at the same time point after ignition, the Peclet number increases with the initial equivalence ratio and shows an increase with higher initial temperatures (but the increase at 300K is not much compared to 360K). A low Peclet number typically corresponds to a smaller flame radius, where the convective effects at the flame front are weaker, resulting in a relatively smooth and stable flame surface. As the flame radius increases, the Peclet number gradually rises, enhancing convective effects and making the flame front more susceptible to disturbances, ultimately leading to the formation of a cellular instability structure.

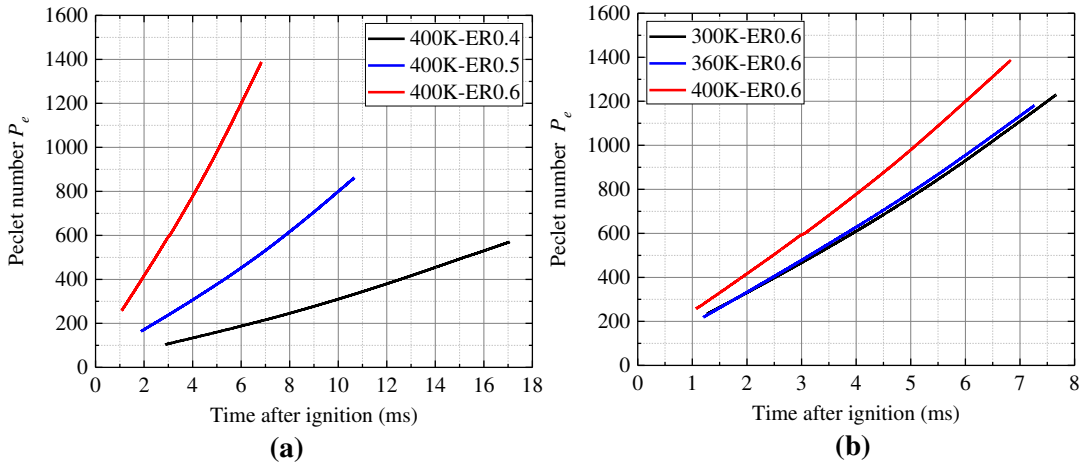

Fig. 7. Peclet number at various temperatures under lean combustion conditions.

3.2 Quantitative characteristics of flame cellularization

Using an in-house developed deep-learning-driven cell detection program, the number and positions of cells on the flame surface were accurately obtained [30]. Figure 8 illustrates the variation in cell number with flame propagation under various initial temperatures in lean combustion conditions. When the flame radius has not yet reached the cellularization critical value, the flame front is primarily characterized by the growth and bifurcation of initial cracks, and the number of cells remains nearly constant. As the flame radius exceeds the critical cellularization radius, cell numbers rapidly increase due to the formation of numerous secondary cracks on the flame surface, which expand to form a cellular structure. It can also be observed in Figure 8 that, under lean combustion conditions, the time at which cell numbers begin to increase is progressively delayed as the equivalence ratio rises, a behavior that differs from results seen under rich combustion conditions [44]. In particular, for an equivalence ratio of ER=0.6, the delay in cell number growth is more pronounced. For ER=0.4 and

0.5, cell numbers become nearly equal when the flame radius reaches approximately 50 mm.

Furthermore, it was observed that even as the flame propagates toward the combustion chamber wall, cell numbers continue to increase, indicating that the flame remains unstable at a radius of 60 mm. Although the chamber wall introduces some interference with flame development, which may cause slight errors in cell count near the wall, the onset time and growth rate of cellularization remain reliable. Additionally, the results show that the trends in cell number variation are similar under initial temperatures of 300 K and 360 K; when the initial temperature increases to 400 K, cell number growth is also delayed, but the growth rate remains high.

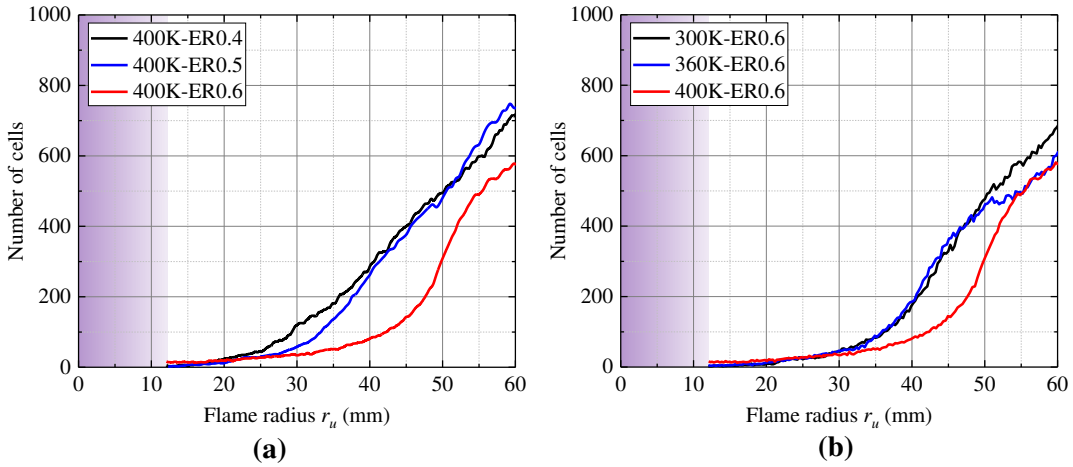

Fig. 8. Cell number at various temperatures under lean combustion conditions.

By conducting 3D reconstruction of all small-scale cells detected by the program [31], the total reconstructed area divided by the number of cells yields the average 3D cell area. Figure 9 presents the evolution of the average 3D cell area on the flame surface under lean combustion conditions and various initial temperatures. The results show that as the flame expands, the average 3D cell area initially increases, then

decreases, and eventually stabilizes within a certain range. Notably, for an equivalence ratio of ER=0.6, the curve exhibits two peaks, which occurs because the rate of cell number increase slows after rapid cellularization of the flame surface, as also evidenced in Figure 8. Additionally, as the equivalence ratio increases, the peak value of the average 3D cell area rises due to the delayed growth in cell number, resulting in relatively fewer cells at the same flame radius. Further analysis reveals that the effect of initial temperature on average 3D cell area is not significant. Under the lean combustion conditions of this study, the final average 3D cell area stabilizes between 30 and 50 mm^2. This indicates that the average cell size has reached a saturation limit, with the interaction between flame propagation and cell division achieving a balance.

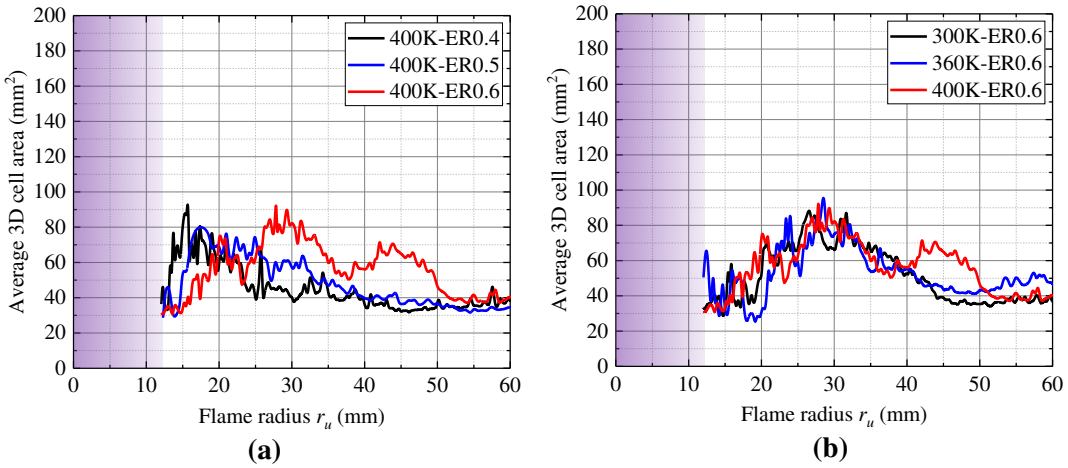

Fig. 9. Average 3D cell area at various temperatures under lean combustion conditions.

Using the in-house developed program to perform 3D reconstruction of cell areas, the cellular flame area under lean combustion conditions and various initial temperatures was obtained, as shown in Figure 10. Under the same flame radius, the cellular flame area provides a direct measure of the wrinkle degree of flame front, indicating the instability level of the flame at that moment. The results show that, during

the early stages of flame development, the influence of different initial equivalence ratios and temperatures on the cellular flame area is minimal due to the initially low degree of cellularization, resulting in only slight differences in flame area. In comparison, under lean combustion conditions with ER=0.4 and 0.5, the flame exhibits a higher degree of cellularization; for ER=0.6, the flame shows more pronounced cellularization at initial temperatures of 300 K and 360 K. These quantitative cellular flame area data will be used in subsequent calculations of the flame self-acceleration exponent, marking the first exploration of the relationship between 3D-reconstructed flame area and flame self-acceleration behavior.

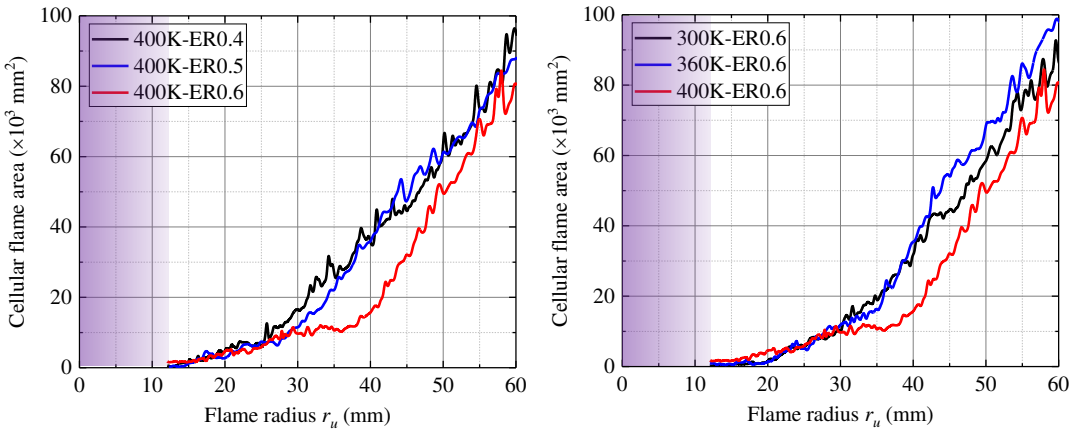

Fig. 10. Cellular flame area at various temperatures under lean combustion conditions.

3.3 Flame self-acceleration analysis

The wave number n is defined as the ratio of the flame circumference to the corresponding wavelength Λ (i.e., cell diameter) at a given moment and serves as a critical parameter for assessing flame instability [42]. For spherically expanding flames, the flame front exhibits a range of wavelengths that may trigger instabilities. The wave

number can be calculated using Equation (6), where δ_k/Λ represents the dimensionless ratio of wavelength to flame thickness.

$$n = 2\pi\frac{P_e}{\Lambda} = 2\pi\frac{r_u}{\delta_k/\Lambda} \quad (6)$$

In cellular instability, the maximum wavelength Λ_{max} (corresponding to the minimum wave number n_{min}) is related to the size of the flame front and represents the longest unstable wavelength that can occur along the flame front, determining the largest scale of flame wrinkling. Conversely, the shortest unstable wavelength Λ_{min} (corresponding to the maximum wave number n_{max}) is primarily influenced by flame thickness and is approximately 50 times the flame thickness [41]. As the spherically expanding flame grows, the range of wavelengths on the flame surface continuously changes. Before the onset of cellular structures, the flame remains stable for all wavelengths [42]; however, once cellular structures start forming on the flame front, the flame cannot maintain stability across all wavelengths, resulting in instability [32].

Figure 11 shows the relationship between wave numbers and Peclet number. The peninsula-shaped region (the shaded area) represents the range of wave numbers at which the flame becomes unstable at a given Peclet number (or flame radius). The leftmost point of the shaded region corresponds to the critical Peclet number, indicating that within the range below this critical Peclet number, the flame is stable for all wavelengths. Once the Peclet number exceeds this critical value, a range of unstable wave numbers appears, showing wave number dependence. Since the maximum wavelength is determined by the size of the flame front, the minimum wave number remains nearly constant, while the minimum wavelength is related to flame thickness,

causing the maximum wave number to increase linearly with Peclet number.

Disturbances due to large wavelengths are stabilized by the stretch effect of the flame, as large wrinkles on the flame front flatten out during flame expansion and disappear over time. Small wavelengths are stabilized by the diffusion effect of the fuel gas, as diffusion tends to reduce temperature and concentration gradients [43]. The results show that the range of unstable wavelengths increases with Peclet number, and this increase in flame wrinkling consequently accelerates flame propagation. Furthermore, the results indicate that under lean combustion conditions, initial temperature has little effect on the wave number distribution in the peninsula-shaped region. With an increase in the initial equivalence ratio, the minimum wave number in the peninsula-shaped region remains unchanged, but the maximum wave number decreases significantly, and the critical Peclet number slightly increases. This is because flames with higher equivalence ratios are more readily stabilized by non-uniform diffusion effects, which impacts the range of unstable wave numbers, a phenomenon that is also verified by the quantitative cellular information of the cellular flame.

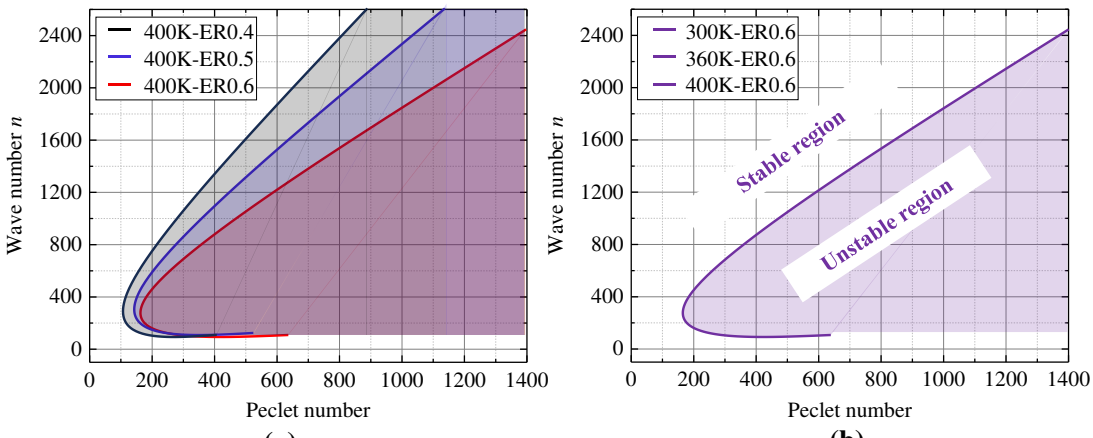

Fig. 11. Wave number at various temperatures under lean combustion conditions.

After the formation of a uniformly distributed cellular structure, the flame

propagation speed (burning velocity) gradually accelerates with increasing combustion time. However, there is still no unified conclusion regarding the acceleration in the flame propagation process. Following the onset of instability, as the flame radius increases, the size of each cell also expands; when the cell size grows too large to counterbalance the effects of instability, cells split into smaller units, and the flame front gradually evolves into a self-similar fractal structure. For spherically expanding fractal flames, this fractal geometric structure is characterized by the flame front being covered with cells of varying sizes. At this stage, the fractal dimension of the flame front, $1 + d$, can be calculated using Equation (7), where d is the fractal excess, A_N represents the cellular flame area, and A_0 is the laminar flame front area at that moment, defined as $A_0 = 4\pi {r_u}^2/3$.

$$A_N = A_0(n_{max}/n_{min})^d \tag{7}$$

Additionally, the self-acceleration exponent a of the cellular flame is directly related to the fractal excess d and can be further calculated using Equation (8) [18]:

$$a = 1/(1-d) \tag{8}$$

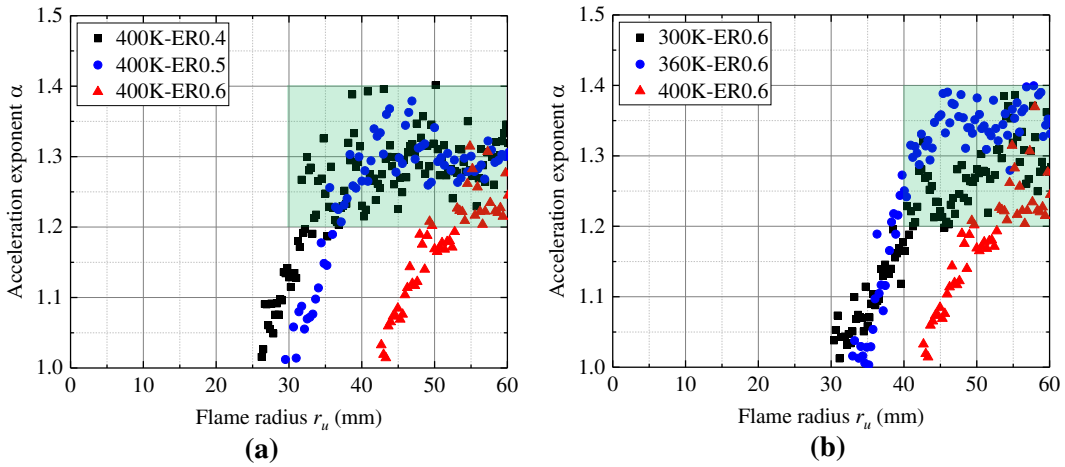

Fig. 12. Acceleration exponent at various temperatures under lean combustion conditions.

The calculated self-acceleration exponent of the flame is shown in Figure 12. When the self-acceleration exponent is greater than 1, the flame exhibits fractal characteristics, with the flame surface rapidly cellularizing and the flame propagation speed increasing significantly over time in a power-law relationship. The experimental setup is compact in this work, with minimal buoyancy effects, making it well-suited for studying the self-acceleration exponent. The results indicate that the self-acceleration exponent is not constant; instead, it increases gradually with flame propagation and eventually stabilizes within a specific range. Under the lean combustion conditions in this study, the self-acceleration exponent stabilizes between 1.2 and 1.4 as the flame propagates to the edge of the viewing window, which is lower than the suggested value for self-turbulence (1.5) [45]. This trend and range align closely with previous fitted results, further confirming the strong correlation between cellular flame area and self-acceleration behavior [20].

4 Conclusions

The self-acceleration of spherically expanding premixed flames is closely related to the cellular area on the flame surface. In this study, the cellular flame area of lean premixed hydrogen-air flames under various initial temperatures was reconstructed in 3D using an in-house image processing program, and the relationship between self-acceleration and quantitative cellular characteristics was further derived. The main findings are as follows:

(1) Raw schlieren images show that with increasing initial temperature and fuel-

air equivalence ratio, the cellularization degree in lean flames tends to decrease.

(2) As the flame radius increases, the stretch rate decreases approximately as a power-law function, with the rate of decrease accelerating with an increase in the fuel-air equivalence ratio, while the effect of initial temperature variations is relatively minor. Overall, higher initial temperatures and greater equivalence ratios lead to higher stretch rates.

(3) With increasing initial equivalence ratio and temperature, the stretched flame propagation speed increases accordingly, though it exhibits low sensitivity to temperature changes. Furthermore, a negative Markstein number indicates high instability to curvature perturbations under ultra-lean conditions (ER<0.5), making the flame surface more prone to cellular structures.

(4) The range of unstable wavelengths increases with Peclet number (flame radius). Under lean combustion conditions, initial temperature has minimal effect on the wave number distribution in the peninsula region. However, with increasing initial equivalence ratio, the minimum wave number remains unchanged, while the maximum wave number decreases significantly, and the critical Peclet number slightly increases.

(5) Under lean combustion conditions, the self-acceleration exponent derived is not constant; instead, it increases gradually with flame propagation and eventually stabilizes in the range of 1.2 to 1.4, which is below the suggested value for self-turbulence (1.5).

Acknowledgements

The authors would like to acknowledge the EPSRC (Engineering and Physical Sciences Research Council, United Kingdom) for the financial support of the project 'Premixed Combustion Flame Instability Characteristics' (Grant No. EP/W002299/1).

Nomenclature

2D	two-dimensional
3D	three-dimensional
ER	equivalence ratios
LED	light emitting diode
HSV	High-speed video
r_u	equivalent flame radius
a	self-acceleration exponents
A	flame area determined by the sum of pixels in binarized image
N	cell number
T	initial temperature
T_{ad}	adiabatic flame temperature
T_u	unburned mixture temperature
$(dT/dx)_{max}$	maximum temperature gradient
r_{cl}	critical radius
α	flame stretch rate
S_n	laminar stretch flame speed
S_L	unstretched flame speed
L_b	Markstein length
M_{ab}	Markstein number

δ_k	flame thickness
P_e	Peclet number
n	wave number
n_{min}	minimum wave number
n_{max}	maximum wave number
Λ	corresponding wavelength (i.e., cell diameter)
Λ_{max}	maximum wavelength
Λ_{min}	shortest unstable wavelength
d	fractal excess
A_N	cellular flame area
A_0	laminar flame front area

References

[1] Zhang G, Shi P, Zhai C, Jin Y, Han M, Liu S, et al. Review of energy self-circulation systems integrating biogas utilization with Powerfuels production in global livestock industry. Bioresource Technology. 2024;408:131193.

[2] Zhang G, Zhang Y, Shi P, Chen P, Schneider L, Xu H, Wu D. Near-field jet characteristics of a single-hole medium-/low-pressure hydrogen injector. Energy. 2025;314:134122.

[3] Kim WK, Mogi T, Dobashi R. Fundamental study on accidental explosion behavior of hydrogen-air mixtures in an open space. International Journal of Hydrogen Energy. 2013;38:8024-9.

[4] Jin Y, Luo H, Zhang G, Zhai C, Ogata Y, Matsumura Y, et al. Ignition timing effect

on the combustion performance of hydrogen addition in methane fermentation gas in a local energy system. Fuel. 2022;324:124714.

[5] Zhang G, Zhang Y, Shi P, Chen P, Schneider L, Xu H, Wu D. Near-field jet characteristics of a single-hole medium-/low-pressure hydrogen injector. Energy. 2025;314:134122.

[6] Figueira da Silva LF. Stochastic characterisation of unstable lean hydrogen–air annular premixed flames. Combustion Theory and Modelling. 2024;28:317-43.

[7] Zhang F, Zhang G, Wang Z, Wu D, Jangi M, Xu H. Experimental investigation on combustion and emission characteristics of non-premixed ammonia/hydrogen flame. International Journal of Hydrogen Energy. 2024;61:25-38.

[8] Liu F, Bao X, Gu J, Chen R. Onset of cellular instabilities in spherically propagating hydrogen-air premixed laminar flames. International Journal of Hydrogen Energy. 2012;37:11458-65.

[9] Goulier J, Comandini A, Halter F, Chaumeix N. Experimental study on turbulent expanding flames of lean hydrogen/air mixtures. Proceedings of the Combustion Institute. 2017;36:2823-32.

[10] Tinaut FV, Reyes M, Melgar A, Giménez B. Optical characterization of hydrogen-air laminar combustion under cellularity conditions. International Journal of Hydrogen Energy. 2019;44:12857-71.

[11] Gostintsev YA, Istratov AG, Shulenin YV. Self-similar propagation of a free turbulent flame in mixed gas mixtures. Combustion, Explosion and Shock Waves. 1988;24:563-9.

[12] Ashurst WT. Darrieus - Landau instability, growing cycloids and expanding flame acceleration. Combustion Theory and Modelling. 1997;1:405-28.

[13] Aldredge RC, Zuo B. Flame acceleration associated with the Darrieus-Landau instability. Combustion and Flame. 2001;127:2091-101.

[14] Bradley D, Cresswell TM, Puttock JS. Flame acceleration due to flame-induced instabilities in large-scale explosions. Combustion and Flame. 2001;124:551-9.

[15] Kwon OC, Rozenchan G, Law CK. Cellular instabilities and self-acceleration of outwardly propagating spherical flames. Proceedings of the Combustion Institute. 2002;29:1775-83.

[16] Gostintsev YA, Fortov VE, Shatskikh YV. Self-Similar Propagation Law and Fractal Structure of the Surface of a Free Expanding Turbulent Spherical Flame. Doklady Physical Chemistry. 2004;397:141-4.

[17] Kim W, Sato Y, Johzaki T, Endo T, Shimokuri D, Miyoshi A. Experimental study on self-acceleration in expanding spherical hydrogen-air flames. International Journal of Hydrogen Energy. 2018;43:12556-64.

[18] Wu F, Jomaas G, Law CK. An experimental investigation on self-acceleration of cellular spherical flames. Proceedings of the Combustion Institute. 2013;34:937-45.

[19] Huo J, Saha A, Ren Z, Law CK. Self-acceleration and global pulsation in hydrodynamically unstable expanding laminar flames. Combustion and Flame. 2018;194:419-25.

[20] Kim W, Namba T, Johzaki T, Endo T. Self-similar propagation of spherically

expanding flames in lean hydrogen–air mixtures. International Journal of Hydrogen Energy. 2020;45:25608-14.

[21] Yang S, Saha A, Wu F, Law CK. Morphology and self-acceleration of expanding laminar flames with flame-front cellular instabilities. Combustion and Flame. 2016;171:112-8.

[22] Huang S, Huang R, Zhang Y, Zhou P, Wang Z, Yin Z. Relationship between cellular morphology and self-acceleration in lean hydrogen-air expanding flames. International Journal of Hydrogen Energy. 2019;44:31531-43.

[23] Xie Y, Elsayed Morsy M, Yang J. Self-Acceleration and global pulsation of unstable laminar Hydrogen-Air flames. Fuel. 2023;353:129182.

[24] Kim WK, Mogi T, Kuwana K, Dobashi R. Self-similar propagation of expanding spherical flames in large scale gas explosions. Proceedings of the Combustion Institute. 2015;35:2051-8.

[25] Bauwens CRL, Bergthorson JM, Dorofeev SB. Experimental investigation of spherical-flame acceleration in lean hydrogen-air mixtures. International Journal of Hydrogen Energy. 2017;42:7691-7.

[26] Bauwens CR, Bergthorson JM, Dorofeev SB. Experimental study of spherical-flame acceleration mechanisms in large-scale propane–air flames. Proceedings of the Combustion Institute. 2015;35:2059-66.

[27] Cai X, Wang J, Bian Z, Zhao H, Dai H, Huang Z. On transition to self-similar acceleration of spherically expanding flames with cellular instabilities. Combustion and Flame. 2020;215:364-75.

[28] Huo J, Saha A, Shu T, Ren Z, Law CK. Self-acceleration and global pulsation in expanding laminar H2-O2-N2 flames. Physical Review Fluids. 2019;4:043201.

[29] Liu Z, Unni VR, Chaudhuri S, Sui R, Law CK, Saha A. Self-turbulization in cellularly unstable laminar flames. Journal of Fluid Mechanics. 2021;917:A53.

[30] Zhang G, Xu H, Wu D, Yang J, Morsy ME, Jangi M, et al. Deep learning-driven analysis for cellular structure characteristics of spherical premixed hydrogen-air flames. International Journal of Hydrogen Energy. 2024;68:63-73.

[31] Zhang G, Xu H, Wu D, Yang J, Morsy ME, Jangi M, Cracknell R. Quantitative three-dimensional reconstruction of cellular flame area for spherical hydrogen-air flames. Fuel. 2024;375:132504.

[32] Bradley D, Harper CM. The development of instabilities in laminar explosion flames. Combustion and Flame. 1994;99:562-72.

[33] Hu X, Luo C, Chen X, Liu Q, Su M. Study on flame propagation and inherent instability of hydrogen/ammonia/air mixture. Fuel. 2024;357:129848.

[34] Bradley D, Gaskell PH, Gu XJ. Burning velocities, markstein lengths, and flame quenching for spherical methane-air flames: A computational study. Combustion and Flame. 1996;104:176-98.

[35] Clavin P. Dynamic behavior of premixed flame fronts in laminar and turbulent flows. Progress in Energy and Combustion Science. 1985;11:1-59.

[36] Bradley D, Hicks RA, Lawes M, Sheppard CGW, Woolley R. The Measurement of Laminar Burning Velocities and Markstein Numbers for Iso-octane–Air and Iso-octane–n-Heptane–Air Mixtures at Elevated Temperatures and Pressures in an

Explosion Bomb. Combustion and Flame. 1998;115:126-44.

[37] Poinsot T, Veynante D. Theoretical and Numerical Combustion: Edwards; 2005.

[38] Xie Y, Elsayed Morsy M, Li J, Yang J. Intrinsic cellular instabilities of hydrogen laminar outwardly propagating spherical flames. Fuel. 2022;327:125149.

[39] Göttgens J, Mauss F, Peters N. Analytic approximations of burning velocities and flame thicknesses of lean hydrogen, methane, ethylene, ethane, acetylene, and propane flames. Symposium (International) on Combustion. 1992;24(1):129-135.

[40] Matalon M. Flame dynamics. Proceedings of the Combustion Institute. 2009;32:57-82.

[41] Bradley D, Sheppart CGW, Woolley R, Greenhalgh DA, Lockett RD. The development and structure of flame instabilities and cellularity at low Markstein numbers in explosions. Combustion and Flame. 2000;122:195-209.

[42] Bechtold JK, Matalon M. Hydrodynamic and diffusion effects on the stability of spherically expanding flames. Combustion and Flame. 1987;67:77-90.

[43] Addabbo R, Bechtold JK, Matalon M. Wrinkling of spherically expanding flames. Proceedings of the Combustion Institute. 2002;29:1527-35.

[44] Bao Y, Li X, Xu C, Wang Q, Oppong F. Experimental and theoretical study of 2-ethylfuran spherical expanding flame: Cellularization, intrinsic instability and self-acceleration. Fuel Processing Technology. 2022;238:107521.

[45] Cai X, Su L, Wang J, Hu E, Huang Z. Cellularity and self-similarity of hydrogen expanding spherical flames at high pressures. Physics of Fluids. 2023;35:064119.

Dear esteemed Editors,

We would like to submit the enclosed manuscript entitled "Relationship investigation between quantitative cellular information and self-acceleration of lean hydrogen-air spherical premixed flame", which we wish could be considered for publication in **Energy**.

Hydrogen energy has gained significant attention in recent years due to its potential as a clean fuel, but its combustion characteristics, particularly flame propagation and explosion safety, remain critical challenges. Due to the high diffusivity of hydrogen molecules, lean hydrogen-air premixed flames are more prone to cellular instability during combustion. This instability is known to often lead to self-acceleration of flame propagation, with the flame speed closely related to the cellular area on its surface. In this study, the relationship between quantitative cellular information and self-acceleration of lean hydrogen-air premixed spherically expanding flames was systematically analyzed under various initial temperatures. Quantitative cellular information, including cell number, two- and three-dimensional average cell area, and total cellular flame area, was obtained using an in-house developed image processing program. Based on these quantitative data, the ratio of cellular flame surface area to laminar flame surface area was calculated, and the fractal dimension of the flame front along with the flame self-acceleration exponent was derived. Results indicate that with increasing equivalence ratio and initial temperature, the onset of cellular instability is delayed, while the self-acceleration exponent gradually increases with flame propagation, eventually stabilizing in the range of 1.2-1.4 after full cellularization (As shown in the Figure below). Under leaner conditions and lower initial temperatures, flames exhibited a higher self-acceleration exponent. The self-acceleration exponent obtained from the 3D-reconstructed cellular flame area offers a new perspective for

developing accurate models of self-accelerating spherically cellular flame propagation, with significant potential applications in hydrogen combustion and explosion safety.

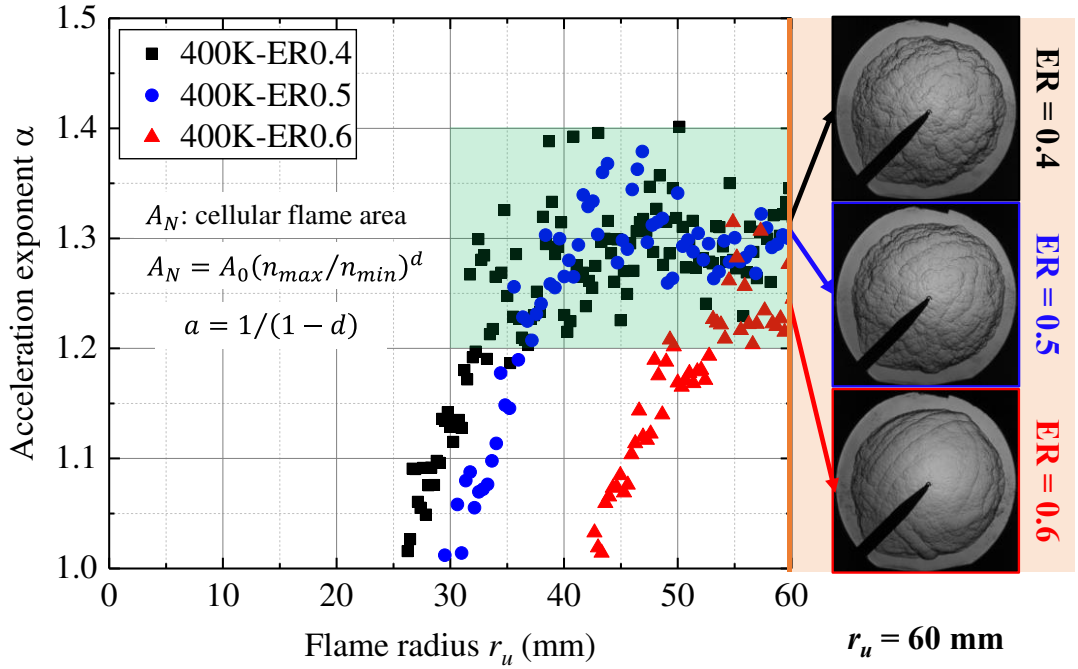

The work described has not been submitted elsewhere for publication, in whole or in part, and all the authors listed have approved the manuscript that is enclosed. We believe that this manuscript will make it interesting to general readers of your journal. We appreciate your consideration of our manuscript, and we look forward to receiving comments from the reviewers. If you have any queries, please don't hesitate to contact me.

Thank you very much for your time and consideration.

Sincerely yours,

Dr. Gengxin Zhang, Research Fellow

Vehicle and Engine Technology Research Centre

Department of Mechanical Engineering, University of Birmingham, UK

Tel: +44 7741 796009 E-mail address: g.zhang.6@bham.ac.uk